Alexandria Engineering Journal (2019) 58, 115–125

HOSTED BY

Alexandria University

Alexandria Engineering Journal

www.elsevier.com/locate/aej
www.sciencedirect.com

ORIGINAL ARTICLE

Minimum transmission power loss in multi-terminal HVDC systems: A general methodology for radial and mesh networks

Sawsan Sayed [a], Ahmed Massoud [b,*]

[a] Department of Electrical Engineering, Qatar University, Doha, Qatar
[b] Department of Electrical Engineering, Qatar University, Doha 2713, Qatar

Received 14 November 2018; revised 5 December 2018; accepted 11 December 2018
Available online 23 December 2018

KEYWORDS

CIGRE B4;
DC voltage droop control;
High-power;
HVDC;
Multi-terminal;
Optimal power flow

Abstract The significant increase of high-power renewable energy sources (e.g., off-shore wind energy systems) in the power networks, has introduced Multi-Terminal High-Voltage DC (MTDC) grids as a prominent approach for transmitting power with high reliability, security, and efficiency. Nonetheless, MTDC systems introduce several challenges pertinent to operation. This paper investigates optimal power flow in MTDC networks to minimize the transmission power loss via DC voltage control, which is an essential approach for the MTDC network operation to maintain the transmission balance and grid stability. In this paper, a generalized approach for minimum transmission power loss in radial and mesh MTDC networks is presented. Voltage droop control is employed in the radial network, with droop characteristics tuned for optimal power flow, which is supported by an optimization approach. Radial MTDC networks with either a common interconnection node or a common interconnection line are considered. While for the mesh network and due to the difficulty of adjusting the droop gains, an optimization algorithm is merely devised for optimal power flow. A modified CIGRE B4 network is employed in this paper to investigate the presented concept considering several scenarios. Simulation results using the Matlab platform are shown to validate the paper's contribution.

1. Introduction

The major benefits of High-Voltage DC (HVDC) transmission can be related to applications of long-distance power transmission systems, asynchronous network interconnection, integration of renewable energy sources, and submarine transmission [1–3]. The HVDC grids have two general interconnections, namely point-to-point HVDC and Multi-Terminal HVDC (MTDC). The MTDC system interconnects more than two DC terminals/nodes, which can be connected as series or parallel (either radial or mesh) configurations [4,5]. The main advantages of MTDC configuration are enhanced reliability, reduced converter stations ratings, ease of maintenance, and energy trading facilitation [4]. In 1987,

* Corresponding author.
E-mail addresses: sa1108530@student.qu.edu.qa (S. Sayed), ahmed.massoud@qu.edu.qa (A. Massoud).
Peer review under responsibility of Faculty of Engineering, Alexandria University.

https://doi.org/10.1016/j.aej.2018.12.007

the first MTDC system was established, and it was based on Line Commutated Converter (LCC) technology [6]. However, the power direction reversal in LCC requires changing the voltage polarity, which involves the complex operation of mechanical switchgear. Thus MTDC network is preferred to be based on Voltage Source Converter (VSC) technology [6–10].

European countries are aiming by 2050 to reduce the gas emissions from greenhouses by 80% through the deployment of renewable energy sources. This can be achieved by upgrading the AC grids with MTDC grids. Several visions for European super DC grid have been investigated. One of these visions is associated with the European Wind Energy Association (EWEA) [11]. Another vision is offered by DESERTEC, which is a global foundation that targets the enormous energy delivered by the sun to the deserts. DESERTEC vision is cooperation expanded between Europe, the Middle East, and North Africa (EUMENA). It is anticipated that the MTDC connection will provide a promising solution for the DESERTEC [12–14].

The power balance in HVDC systems is a key factor for the stability of the network. Due to the limited stored energy in the DC grid, typically the stored energy in the DC capacitors and lines, the DC voltages of the system change fast. Thus, the power balance in MTDC systems reflects on the DC voltage [15]. The coordination and management between the generation and demand terminals in the MTDC network are achieved through hierarchical control layers [15]. Fig. 1 shows a general illustration of the hierarchical control layers in MTDC network [16] and the time constant for the control layers are shown [17]. The VSCs that receive power in the MTDC grid have a primary controller to adjust their injected power. The secondary controller adjusts the power-sharing among converters according to the scheduled power exchange considering Optimal Power Flow (OPF) in the DC grid (e.g., minimizing the resistive losses in the network). In addition, a tertiary control center allows redistribution of the power references according to the restrictions and requirements of the DC grid in different areas [15]. Further elaboration on MTDC network control layers integration is provided in [17,18].

In two-terminal HVDC-VSC, one converter controls the active power, while the other converter controls the DC voltage. However, in MTDC networks, controlling the DC voltage through only one converter has significant drawbacks due to the limited power rating of the converter responsible for controlling the DC voltage [19]. Several control techniques have been investigated for power flow control in MTDC networks, such as master-slave, voltage margin, voltage droop, and hybrid control techniques combining both voltage margin and voltage droop control.

In master-slave control, the master converter is the DC slack terminal that manages any imbalance occurring overall the network, such that it absorbs or injects the power to achieve DC system balance, while the operation of the remaining converters is based on constant power mode. However, losing the slack terminal will cause DC network instability, which is the main disadvantage of this technique [20,21]. The voltage margin control method is as an extension to the master-slave control, such that the voltage control is shared among the converters according to their reference voltages and power levels. In this method also the DC voltage control of the whole network depends on one converter at a time [19]. The main draw-

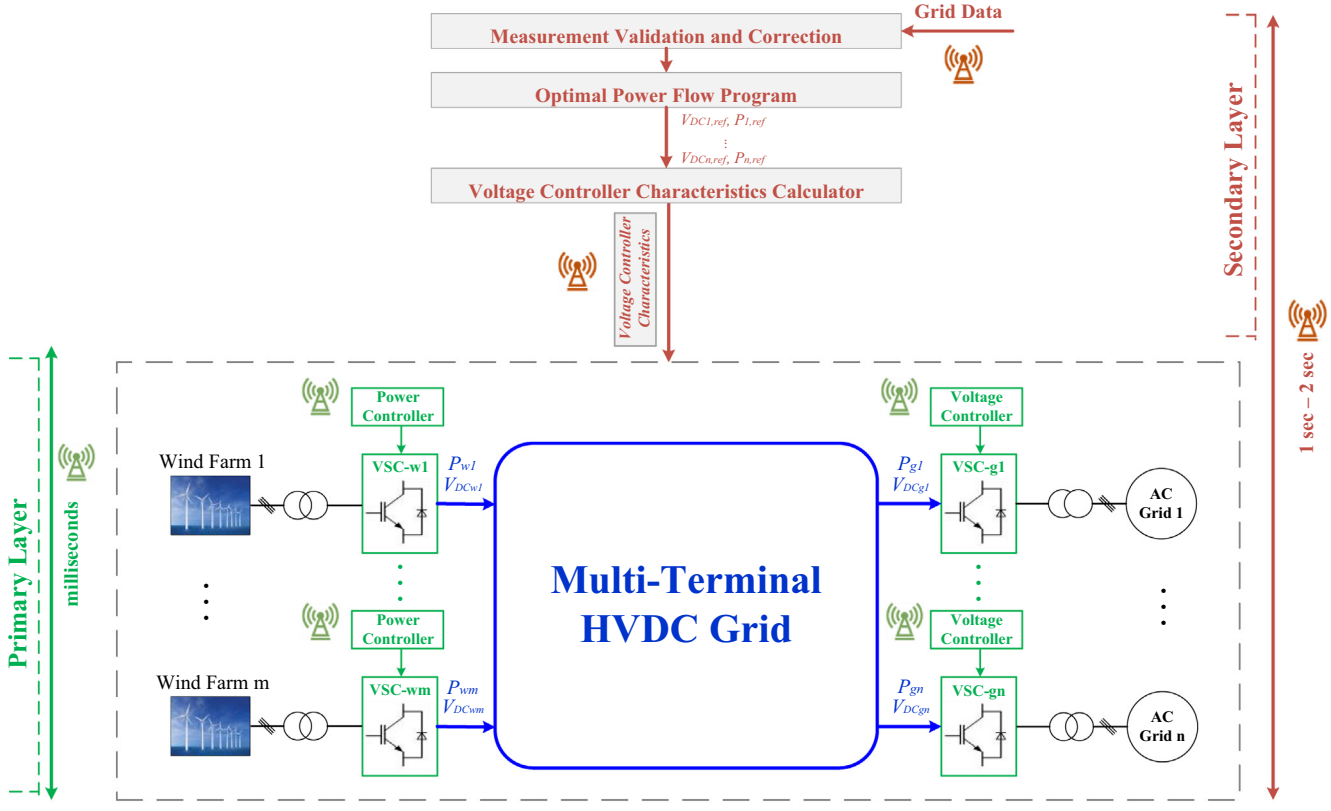

Fig. 1 A general overview of the hierarchical control in multi-terminal HVDC-VSC networks.

back of this method is the high-voltage oscillations resulting from swapping of the DC voltage control among the converters [19].

The voltage droop-based control method is a common control approach in MTDC network. It allows converters power-sharing and exchange according to the droop characteristic without communication requirements [21–23]. Yet, the selection of the droop gains is not always straightforward, and fixed droop characteristics have issues during MTDC network disturbance events (i.e., converter outage, network line reconfiguration, and power injection fluctuation) [24]. To overcome the fixed droop control issues, distributed voltage control or adaptive droop control methods are introduced. With these two methods, the reference points and control parameters are computed periodically by the secondary controller and communicated to the converters [19]. With input power variation, droop control ensures only sub-optimal power flow. Nonetheless, OPF for minimum power loss can be guaranteed through hierarchical control layers with input power variations.

In addition to power-sharing facilitation, OPF in steady-state can be achieved by proper droop characteristic design to obtain auxiliary functions [25,26], as high dynamic performance [27], post-outage power redistribution [28,29], and transmission loss minimization [21,26,30,31]. Moreover, several studies have presented approaches for the selection of the droop characteristics to achieve optimal DC voltage dynamics in MTDC networks [32–34]. Yet, a general approach that considers both radial and mesh MTDC networks for minimum transmission power loss in the context of hierarchical control, complying with system constraints, needs to be comprehensively addressed.

This paper focuses on DC transmission line power loss minimization in MTDC network with radial and mesh configurations. Optimized droop-controlled MTDC network design for minimum transmission loss has been introduced in [21] with optimal droop characteristic, and it was extended to address adaptive droop control in [26]. However, this was only limited to a particular radial interconnection with a common interconnection node (i.e., common interconnection line has been discarded). Distributed voltage control with optimization approach for minimizing the DC grid losses in radial MTDC has been presented in [35]. However, communication loss may lead to critical network operation compared to droop-controlled MTDC system. In [30,31], an optimization algorithm has been presented for minimum power loss in radial and mesh MTDC networks. However, the DC voltage droop characteristics design for proper power-sharing has not been elaborated. Further studies address OPF for transmission loss minimization considering both high-voltage AC and DC grids through central controller algorithms [36,37]. All these studies have not illustrated a generalized interconnection classification for radial MTDC network power loss minimization. The optimization techniques provided for MTDC network in [30,31] can be extended for general radial and mesh interconnection in MTDC networks, however, OPF is not guaranteed without communication.

In this paper, a generalized approach considering radial and mesh MTDC networks for minimum transmission system losses is presented. Voltage droop control is used in the radial network, with droop characteristics adjusted for OPF, which is supported by an optimization approach. Radial MTDC networks with either a common interconnection node or a common interconnection line are considered. While for the mesh network and due to the difficulty of adjusting the droop gains for minimum power loss, an optimization algorithm is merely employed. DC voltage control and optimal power-sharing for MTDC network are demonstrated using a modified CIGRE B4 network. The network entails three configurations: point-to-point, radial, and mesh. Generally, three case studies are illustrated for HVDC-VSC network. The main contribution of the paper can be summarized as follows:

- Providing a generalized approach for voltage droop control-based OPF in radial MTDC networks with either a common interconnection node or a common interconnection line.
- Providing an optimization approach for OPF of both radial and mesh MTDC networks.
- Validating the presented concept for both radial and mesh MTDC networks through a modified CIGRE B4 system.

The following section delivers further information pertinent to the CIGRE B4 system as a benchmark. Section 3 addresses the design of the droop controller and the optimization approach. Section 4 presents the results of the case studies. Finally, the conclusion of the paper is elucidated in Section 5.

2. Modified CIGRE B4 system

In order to provide a unified test platform for HVDC grids, the International Council on Large Electric Systems (CIGRE) has developed benchmark models to provide a common reference to the researchers to verify the performance and characteristics of the control actions and protection strategies [38,39]. The Working Group 14.02 of CIGRE has developed the first CIGRE HVDC grid benchmark in 1991, which was a test model for different HVDC control schemes. This test model is a point-to-point HVDC network based on LCC technology [39]. CIGRE has developed another test model in 2013, the CIGRE B4 DC grid system, through Working Groups B4-57 and B4-58. A modified CIGRE B4 is shown in Fig. 2, where the detailed configuration and data are presented in [39].

The modified CIGRE B4 system consists of eleven AC-DC converters with three main subsystems, namely a point-to-point HVDC-VSC link, a radial system of 4-terminal HVDC-VSC, and a mesh system of 5-terminal HVDC-VSC. Through the following section, the DC voltage control and OPF for these subsystems are elaborated. The minimization of the power losses in the MTDC network may include the transmission lines losses and the converters losses as shown in (1) [31].

$$[MIN]P_{Loss} = \alpha P_{Loss,line} + \beta P_{Loss,conv} \tag{1}$$

Where $P_{Loss,line}$ is the DC transmission lines losses as shown in (2). $P_{Loss,conv}$ is the VSCs losses as shown in (3).

$$P_{Loss,line} = \sum_{i=1}^{n} \sum_{j=1}^{m} G_{ij}(V_i - V_j)^2 \tag{2}$$

Where G_{ij} is the line conductance between node voltage V_i and V_j, and the indices n and m refer to the number of con-

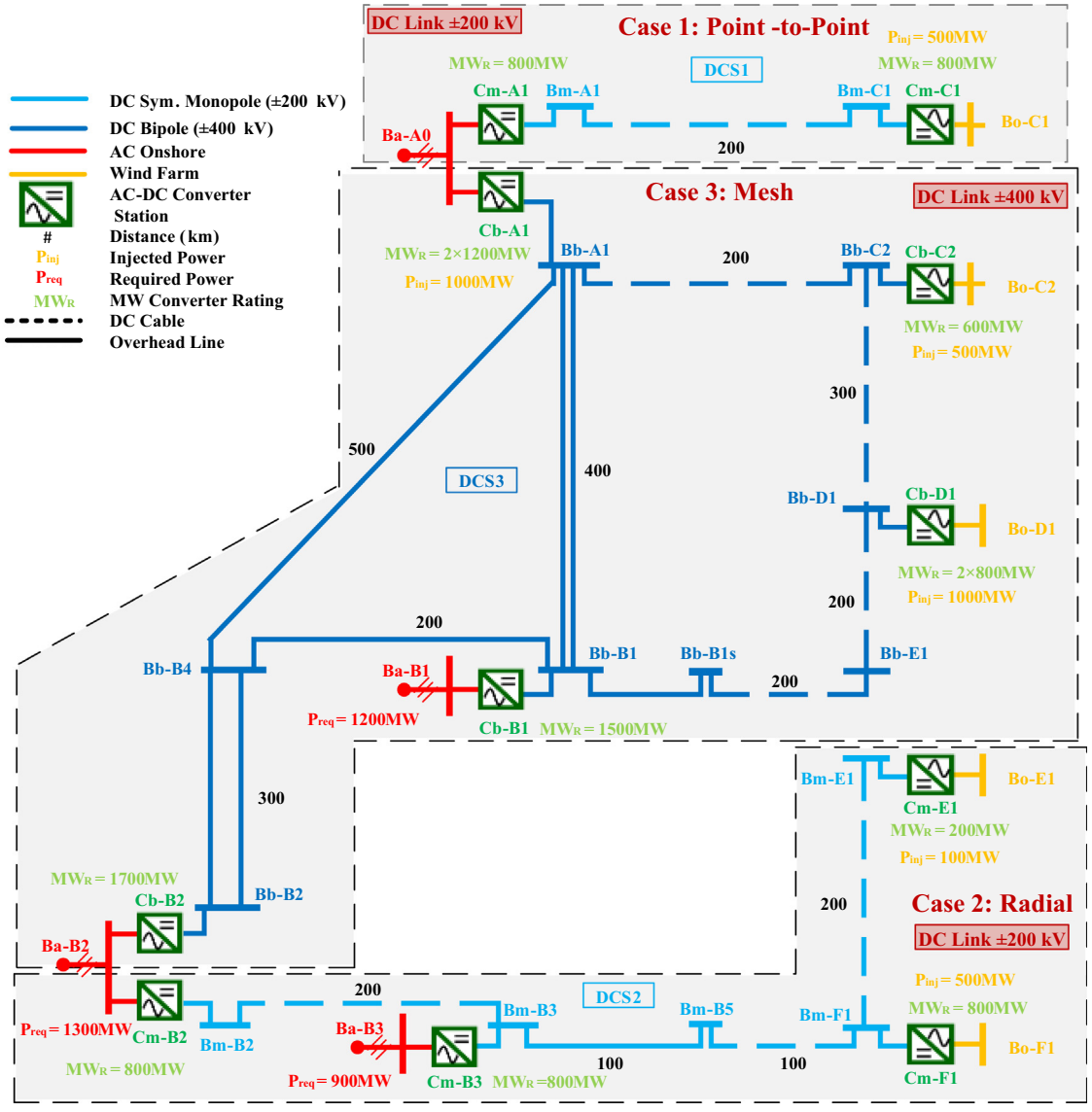

Fig. 2 Case studies on the modified CIGRE B4 HVDC-VSC system.

verters responsible of injecting and receiving the power, respectively.

$$P_{Loss,conv} = \sum_{i=1}^{s} R_a + R_b I_{ac,i} + R_c {I_{ac,i}}^2 \tag{3}$$

Where the no-load losses, linearly dependent losses, and the quadratically dependent losses are represented by R_a, R_b, and R_c, respectively, for s VSC in the MTDC network. Nevertheless, estimating these parameters is challenging, especially in high-voltage high-power applications. $I_{ac,i}$ is the AC current flowing through the i^{th} converter. The AC side power flow is not considered in this paper (i.e., only the DC side power flow is considered). Therefore, the power loss minimization in the MTDC network will be deliberated in (1) while setting $\beta = 0$.

3. DC voltage control and optimal power flow

3.1. Case study 1: Point-to-point HVDC-VSC

The first case involves a point-to-point HVDC-VSC network, with the configuration shown in Fig. 2. A total power of 500 MW is injected by the wind farm. In this case, the converter connected to the wind farm side controls the active power. While the grid-side converter controls the DC voltage. The point-to-point HVDC-VSC connection has been addressed thoroughly in the literature [35,40].

3.2. Case study 2: Radial MTDC

The second case study is a radial network, as shown in Fig. 2. The network is a four-terminal HVDC-VSC, with two wind farms injecting a total power of 600 MW, and two receiving

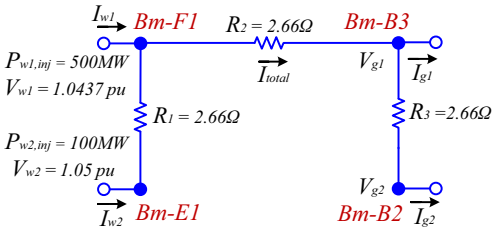

Fig. 3 Modified CIGRE B4 4-terminal radial network equivalent DC circuit, where Bm-F1 is the 1st wind-side converter terminal, Bm-E1 is the 2nd wind-side converter terminal, Bm-B3 is the 1st grid-side converter terminal that is connected to grid 1, and Bm-B2 is the 2nd grid-side converter terminal that is connected to grid 2.

Table 1 Modified CIGRE B4 radial network ratings, where P_{wi} is the power rating of the i^{th} wind-side converter, and P_{gi} is the power rating of the i^{th} grid-side converter.

Parameter	Rating	
Converter power limit	P_{w1}, P_{g1}, P_{g2}	$800MW$
	P_{w2}	$200MW$
Lines current limit	$3000A$	
DC link voltage	$\pm 200kV$	

ends AC grids. The 4-terminal HVDC-VSC radial network DC equivalent circuit is shown in Fig. 3, and the network ratings are presented in Table 1.

The converters have different operating modes according to their functionality. If the converter injects power to the HVDC network (wind-side converter), then during normal network operation, the converter operates in constant power mode such that the maximum/available power generated from the wind farm is injected into the MTDC network. Otherwise, during network disturbance, the converter acts in current limit or droop control modes according to the network condition. The mathematical representation of these modes is presented in (4), where V_w is the terminal DC voltage, I_w is the DC current, V_{wH}/V_{wL} are maximum/minimum terminal voltages, I_{wH} is the maximum current capability of the converter, and K is the droop constant [21].

$$I_w = \begin{cases} (V_{wH} - V_w)/K, & V_{wL} < V_w < V_{wH} \\ \frac{P_w}{V_w}, & V_w < V_{wL} \ and \ I_w < I_{wH} \\ I_{wH}, & I_w \geq I_{wH} \end{cases} \quad (4)$$

While if the converter receives power from the MTDC network (grid-side converter), then the converter acts in DC voltage droop control mode. Otherwise, during network disturbance, the converter acts in current limit mode [21]. The mathematical representation of these modes is presented in (5), where K is the droop constant, V_g is the converter terminal DC voltage, V_{gL} is the no-load DC voltage of the network, and I_{gH} is the maximum current capability of the converter. The DC voltage is controlled with droop constant in terms of the grid DC current, I_g.

$$I_g = \begin{cases} (V_g - V_{gL})/K, & I_g < I_{gH} \\ I_{gH}, & otherwise \end{cases} \quad (5)$$

The maximum DC current of the converter can be expressed as in (6) in terms of the AC grid voltage, V_{AC}, and maximum rated AC current, $I_{AC,max}$ assuming a unity power factor (considering the maximum power capability of the converter $P_{max} = 3V_{AC}I_{AC,max}$).

$$I_{gH} = \frac{P_{max}}{V_g} \quad (6)$$

For the 4-terminal radial network shown in Fig. 3, normal operation is considered for the converters with OPF. The radial network with OPF operation can be divided into three scenarios as presented in Fig. 4 and elaborated in the flowchart of Fig. 5. These scenarios take into consideration that the total generated power from the wind farms is lower than the required grid power. While in case if the total generated power from the wind farms is higher than the required grid power, then the pitch angle of the wind turbines is controlled to reduce the injected power to the radial network [41,42]. Nevertheless, to avoid the possibility of overvoltage that might be experienced at the MTDC nodes, either storage element may be utilized (e.g. flywheel storage system) or the surplus transient power will be dissipated in DC damping resistors [43].

- Scenario 1: Considering that the entire power injection by the wind farms is within the converter rating of grid 1. Then the total power is transmitted to grid 1 for minimum transmission power loss. That is to avoid additional losses by R_3, assuming that the transmission system operator has no further preferences. Thus grid 1 converter operates in DC voltage control mode. While grid 2 does not receive any power.
- *Scenario 2:* If the total power injected by the wind farms exceeds the converter rating of grid 1, then the extra power is received by grid 2. Grid 1 operates in constant power mode. While grid 2 operates in DC voltage control mode.

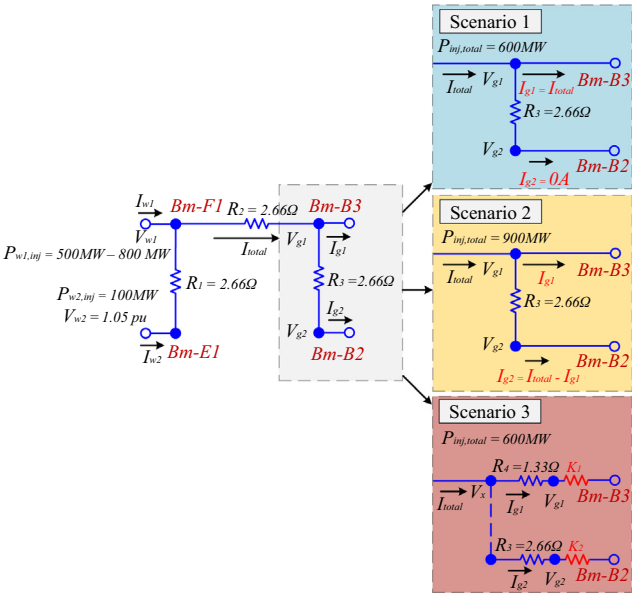

Fig. 4 OPF scenarios for the modified CIGRE B4 4-terminal radial network, where $P_{inj,total}$ is the total power injected by the wind-side converters.

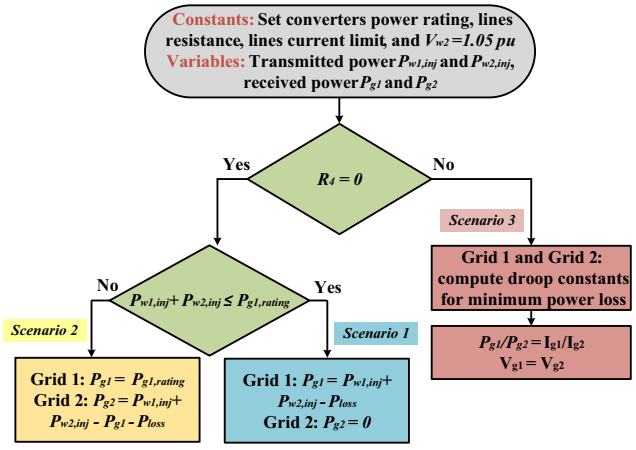

Fig. 5 Flowchart elaborating the radial network scenarios for OPF, where R_4 is the transmission line resistance for the grid with terminal Bm-B3, $P_{wi,inj}$ is the injected power by the i^{th} wind-side converter, P_{gi} is the power received by the i^{th} grid-side converter, $P_{gi,rating}$ is the power rating of the i^{th} grid-side converter, P_{loss} is the radial network total transmission power loss, I_{gi} is the current injected to the i^{th} grid-side converter, and V_{gi} is the terminal DC voltage of the i^{th} grid-side converter.

- *Scenario 3:* The last scenario considers a transmission line for the connection to grid 1 (i.e., a non-zero resistance R_4), then the OPF with droop control for minimum power loss is achieved under two conditions according to [21]. That is the grid-side converters terminal DC voltages are equal, and the power distribution among the converters is inversely proportional with their line resistances.

Generally, OPF, with droop characteristics for minimum power loss design at the grid-side converters, is summarized through the flowchart shown in Fig. 6, which can be explained as follows:

A general interconnection for radial MTDC network with minimum transmission loss condition is elaborated in the following sections.

3.2.1. Radial MTDC networks with a common interconnection line

Minimum power loss condition in radial MTDC networks considering a common interconnection line (shown in Fig. 7) can be clarified as follows.

In order to ensure the minimum power loss condition, the steps introduced in the flowchart in Fig. 6 for the sending end terminals will be followed. Yet, at the receiving end terminals, the power loss can be expressed as:

$$P_{loss} = R_3(I_{w1} - I_x)^2 + R_4(I_{w2} + I_x)^2 + R_x I_x{}^2 \tag{7}$$

For minimum power loss (i.e., considering $\frac{\partial P_{loss}}{\partial I_x} = 0$)

$$I_{g3} = (I_{w1} - I_x) = \frac{I_{w1}(R_x + R_4) + I_{w2}R_4}{R_3 + R_4 + R_x} \tag{8}$$

$$I_{g4} = (I_{w2} + I_x) = \frac{I_{w2}(R_x + R_3) + I_{w1}R_3}{R_3 + R_4 + R_x} \tag{9}$$

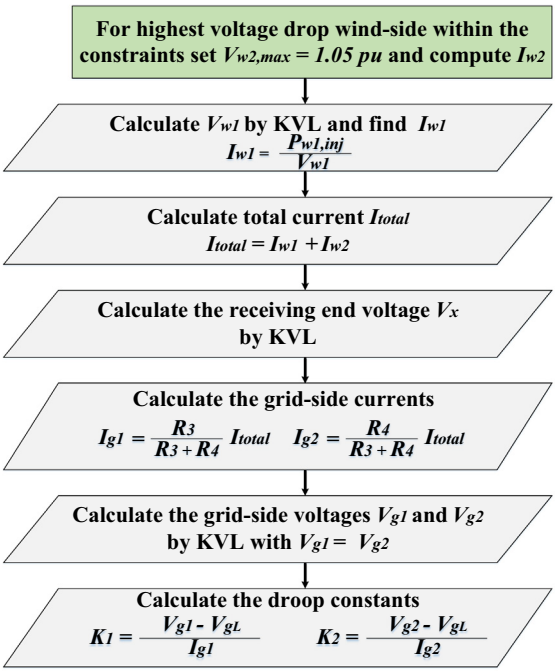

Fig. 6 Flowchart for optimal droop characteristics design for modified CIGRE B4 radial network scenario 3, where V_{wi} is the terminal DC voltage of the i^{th} wind-side converter, I_{wi} is the current injected by the i^{th} wind-side converter, and $P_{wi,inj}$ is the power injected by the i^{th} wind-side converter.

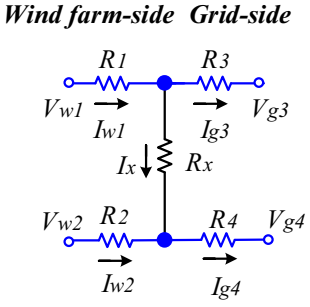

Fig. 7 Radial MTDC network with a common interconnection line.

3.2.2. Radial MTDC networks with a common interconnection node

If the radial MTDC network is with a common interconnection node (i.e., R_x in Fig. 7 is set to zero), in this case, it can be seen that the condition presented in [21] is achieved where the currents I_{g3} and I_{g4} are found as. $I_{g3} = \frac{R_4}{R_3+R_4} I_{total}$ and $I_{g4} = \frac{R_3}{R_3+R_4} I_{total}$where $I_{total} = I_{w1} + I_{w2}$. This can be obtained through substituting $R_x = 0$ in (8) and (9).

3.2.3. Optimal power flow

Referring to the flowchart in Fig. 6 and through all the scenarios for OPF, the terminal Bm-E1 is assumed with voltage $V_{w2} = 1.05pu$, thus, the injected current from this wind farm

is $I_{w2} = 0.476kA$. This converter is chosen due to having the highest voltage drop at the common-point. This guarantees minimizing the current, therefore increasing the network efficiency. The normal operating bands for the DC voltage is typically between 5% and 10% deviation from the nominal value [30,37,44]. For MTDC network steady-state operation, a 5% voltage deviation is considered in order to set a reserve for dynamics operations [18]. In scenarios 1 and 3 in Fig. 4, the wind farms total power injection is 600 MW. Therefore, the voltage at Bm-F1 is found as 1.0437pu. While the injected current from the wind farm connected to Bm-F1 is found as $I_{w1} = 2.395$kA. Correspondingly, the total current flowing to the grid-side is$I_{total} = 2.871$kA. The grid-side DC voltage for scenario 1 at Bm-B3 is computed as 1.005pu by current flow equation between V_{w1} and V_{g1} as shown in (10).

$$V_{g1} = V_{w1} - I_{total}R_2 \tag{10}$$

While for scenario 3, solving KVL for the grid-side converters voltages, V_{gi} for $i = 1, 2$, the receiving node voltage, V_x as shown in (11), and using the currents for minimum loss, the condition shown in (12) is obtained for OPF with minimum transmission power loss [21].

$$V_{gi} = V_x - I_{gi}R_{gi} \tag{11}$$

$$V_{g1} = V_{g2} \tag{12}$$

Where I_{gi} is the current injected to the i^{th} grid-side converter. R_{gi} is the transmission line resistance of the i^{th} grid-side converter.

Generally, for droop-controlled radial MTDC network with n grid-side terminal, with a common interconnection node configuration, the OPF for minimum transmission loss is achieved with the conditions shown in (13) and (14) [26], for $i = 1, 2, \cdots, n$.

$$I_{gi} = \frac{\frac{1}{R_{gi}}}{\sum_{i=1}^{n}\frac{1}{R_{gi}}} I_{total} \tag{13}$$

$$V_{gi} = V_{gth} = I_{total}\frac{1}{\sum_{i=1}^{n}\frac{1}{R_{gi}}} \tag{14}$$

Where I_{total} is the total current injected by the wind-side converters. V_{gth} is the equivalent DC voltage of the grid-side converters. R_{gi} is the transmission line resistance of the i^{th} grid-side converter.

For scenario 2, the total power injection is 900 MW such that the grid-side converter for grid 1 receives 800 MW, that is the maximum power capability of the converter. While the rest of the power injection is received by the grid-side converter of grid 2.

The network analysis and validation of the results for these scenarios are presented in Section 4.

3.3. Case study 3: Mesh MTDC

The third case study considers the mesh five-terminal DC network shown in Fig. 2. In this case, optimization for obtaining minimum transmission power loss is employed. Communication loss between the control layers during normal operation with variable power injection leads to not operating at minimal power loss. While in the case of radial droop-controlled MTDC network, sub-optimal power flow is preserved due to the optimal droop characteristics design [30]. The general objective function for HVDC transmission losses can be written as shown in (2).

The modified CIGRE B4 HVDC mesh network consists of two wind farms injecting a total power of 1500 MW, and AC grid injecting 1000 MW. Two AC grids, denoted with terminal Bb-B1 and Bb-B2, receive the injected power to the MTDC network with OPF. The total power loss in the DC transmission lines for mesh network is represented by (15). The line conductances and node voltages are clarified in the DC equivalent circuit of the 5-terminal HVDC-VSC mesh network shown in Fig. 8. The mesh system ratings are presented in Table 2.

$$\begin{aligned} P_{Loss} = {} & G_1(V_{w2} - V_{w1})^2 + G_2(V_{w2} - V_{g1})^2 + G_3(V_{w1} - V_{gs})^2 \\ & + G_4(V_{g1} - V_{gs})^2 + G_5(V_{g1} - V_m)^2 \\ & + G_6(V_{gs} - V_m)^2 + G_7(V_m - V_{g2})^2 \end{aligned} \tag{15}$$

The total power loss minimization is achieved by obtaining a set of node voltages in the MTDC grid subject to specific system constraints that will acquire the OPF. In order to maintain the condition of OPF with minimum power loss, the sending

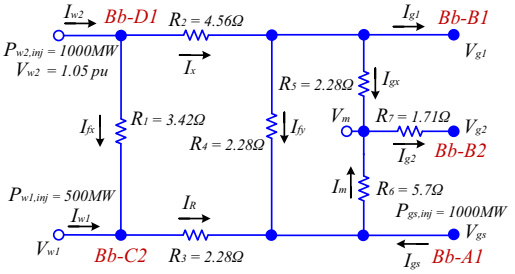

Fig. 8 Modified CIGRE B4 5-terminal mesh network equivalent DC circuit, where Bb-C2 is the 1st wind-side converter terminal, Bb-D1 is the 2nd wind-side converter terminal, Bb-A1 is the converter terminal for the AC grid that injects power to the mesh network, Bb-B1 is the 1st grid-side converter terminal, Bb-B2 is the 2nd grid-side converter terminal, $P_{wi,inj}$ is the power injected by the i^{th} wind-side converter, and $P_{gs,inj}$ is the power injected by the AC grid at terminal Bb-A1.

Table 2 Modified CIGRE B4 mesh network ratings, where P_{wi} is the power rating of the i^{th} wind-side converter, P_{gi} is the power rating of the i^{th} grid-side converter, and P_{gs} is the power rating of the converter connected to terminal Bb-A1.

Parameter	Rating	
Converter power limit	P_{w1}	$600MW$
	P_{w2}	$1600MW$
	P_{gs}	$2400MW$
	P_{g1}	$1500MW$
	P_{g2}	$1700MW$
Lines current limit	$3500A$	
DC link voltage	$\pm 400kV$	

end terminals should operate at their voltage limit. The line of highest voltage drop is chosen to be controlled at 1.05pu as per the constraint in (16) [45].

$$\begin{aligned} 0.95\text{pu} \le V_{DC} \le 1.05\text{pu} \\ -I_{DC,\text{Line},min} \le I_{DC,Line} \le I_{DC,\text{Line},max} \\ 0 \le P_{DC} \le P_{DC,max} \end{aligned} \tag{16}$$

Where V_{DC} is a node DC voltage in the MTDC network. $I_{DC,Line}$ is the DC current flow in the MTDC network lines. $I_{DC,\text{Line},max}$ and $I_{DC,\text{Line},min}$ are the DC lines current maximum/minimum limit. P_{DC} is the power injected or received by a converter in the MTDC network. $P_{DC,max}$ is the maximum converter power capability.

As shown in (15), the OPF is defined by nonlinear function, in terms of node voltages, with the constraints presented in (16). While the power and current operation ranges, shown in (16), are expressed as non-equality constraints [37]. The power limits are taken as the converter maximum ratings, and the current limits are taken as the maximum/minimum DC lines limit.

Classical optimization techniques such as linear and nonlinear programming are suitable methods for special cases and may lead to local optimal solutions. The existence of systems with complex optimization problems incorporating uncertainties has led to the development of metaheuristic optimization methods [46]. Metaheuristic algorithms, as Genetic Algorithm (GA), are suitable for searching the near-optimal solutions while avoiding local solutions by introducing randomization to the search process [46]. Further elaboration on the fundamentals and types of the metaheuristic optimization are presented in [46–49]. Matlab optimization toolbox is available for solving nonlinear equations and constraints, in particular, the GA function, which is used in this case. The optimization approach minimizes the objective function to obtain the optimal points for its variables, such that the objective function is the power losses in the DC lines as shown in (15). Therefore, the power losses in the DC lines are minimized. In addition, the objective function is subjected to some constraints, such as the voltage, current, and power capability of the converters and DC lines, as shown in (16), for the stability of the network. Moreover, constraints are considered for the current flow through the lines as KCL equations at the nodes of interconnection between the lines, as shown in (17). The KCL equations are elaborated considering the mesh network shown in Fig. 8.

$$\begin{aligned} I_{fx} - I_{w2} + I_x = 0 \\ I_{fx} + I_{w1} - I_R = 0 \\ I_R + I_{fy} - I_m + I_{gs} = 0 \end{aligned} \tag{17}$$

For efficient power flow, the highest voltage drop wind farm terminal is assumed at the highest DC voltage within the limit, such that the second wind-side converter is chosen with $V_{w2} = 1.05$pu. In case V_{w1} is assigned with the maximum allowed voltage limit, over-voltage occurs at V_{w2}. Accordingly, the current injected from the second farm is 2.381kA. Additional two constraints are taken into consideration. These constraints are load flow equations for the unknown node voltages, which inject power to the network, V_{w1} and V_{gs}. The two constraints are imposed in terms of the power injections of each terminal. The results of OPF in this case is shown in the following section.

4. Results and discussion of the case studies

This section shows the results of the case studies in Fig. 2. The point-to-point case will not be considered here, as the concept of operation has been elaborated previously in the literature. The results for the 4-terminal radial network scenarios are shown in Fig. 9.

For the first scenario, grid 1 receives the total current generated by the wind farms. Thus, $I_{g2} = 0$A as shown in Fig. 9 (a). While in the second scenario as shown in Fig. 9 (b), the total injected power increases to 900 MW. Thus, grid 1 receives 800 MW which is its maximum capability for minimum power loss, then the rest of the power is received by grid 2. The grid-side converter for grid 2 operates in DC voltage control mode

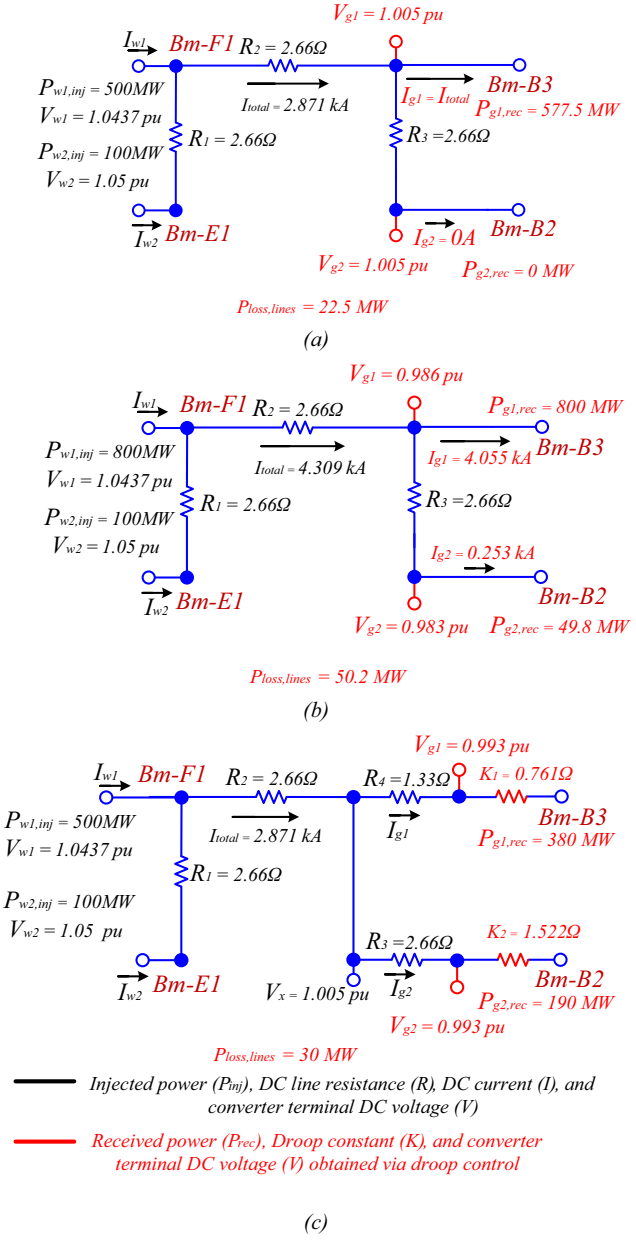

Fig. 9 Radial network OPF analytical results for minimum power loss (a) Scenario 1, (b) Scenario 2, (c) Scenario 3.

to regulate the network voltage. It can be seen that the additional power introduced higher power losses compared to scenario 1. According to Table 1, the line current limit is 3 kA. However, this is considering symmetrical monopole converter configuration (i.e., two HVDC lines). Therefore, the total current through R_2 is within the line current capability. The droop constants of the third scenario are calculated using Fig. 6. The droop constants are calculated by finding the injected currents with minimal power loss. OPF with minimal transmission loss is maintained as long the droop constants are fixed to the shown values in Fig. 9 (c).

Furthermore, Matlab optimization toolbox, GA, is used for the radial network scenarios. The optimum operating voltage points, power received by the converters, and the total power loss in the network match the analytical results obtained in Fig. 9.

The objective function for the first two scenarios of the radial network is shown in (18).

$$P_{Loss} = G_1(V_{w2} - V_{w1})^2 + G_2\left(V_{w1} - V_{g1}\right)^2 + G_3(V_{g1} - V_{g2})^2 \tag{18}$$

While the constraint for these two scenarios is shown in (19).

$$I_{g1} + I_{g2} - I_{total} = 0 \tag{19}$$

Grid 1 in scenario 2 operates in its maximum power capability. Thus, an additional constraint is considered as shown in (20). Where the 1st grid-side converter rating is $P_{g1,rating}$ = 800MW.

$$\frac{P_{g1,rating}}{V_{g1}} - I_{g1} = 0 \tag{20}$$

The optimization objective function for the third scenario of the radial network is shown in (21).

$$P_{Loss} = G_1(V_{w2} - V_{w1})^2 + G_2(V_{w1} - V_x)^2 + G_3(V_x - V_{g2})^2 + G_4(V_x - V_{g1})^2 \tag{21}$$

While the constraint for this scenario is the same as the previous scenarios, as shown in (19). The unknown currents that are I_{g1} and I_{g2} are declared in terms of the network voltages as per the optimization function variable. The constraints presented in (16) are also considered for all the scenarios of the radial network.

Fig. 10 shows the results for applying the optimization approach to the 5-terminal mesh HVDC-VSC network.

As shown, the converter terminal DC voltage for the wind farm connected to Bb-D1 is assumed 1.05pu, while the other node voltages are obtained via the optimization approach. The voltages are constrained by ±5% around the nominal value. The terminal Bb-B1 receives most of the injected power for OPF compared to the terminal Bb-B2. The constraints of the power and current ratings of the converters and DC lines as shown in Fig. 10 are confirmed according to Table 2. Accordingly, the DC grid voltages and currents flow for OPF are obtained as shown in Fig. 10.

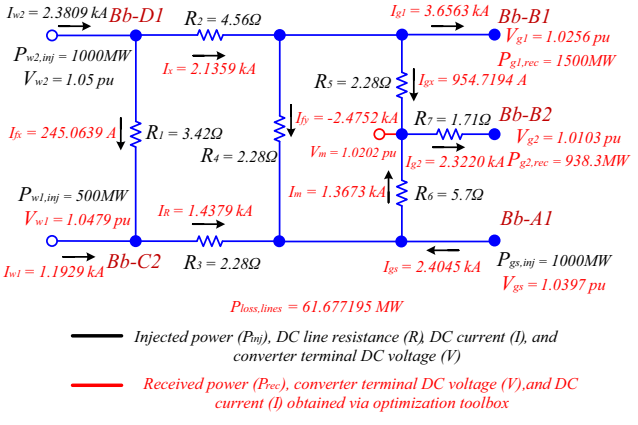

Fig. 10 Mesh network optimization results for OPF.

5. Conclusion

This paper presents a generalized approach for OPF with minimal transmission power loss in radial and mesh MTDC networks. Voltage droop control is applied for the radial network, which guarantees stable DC voltage for the system with droop characteristics that maintains sub-optimal power flow in case of normal network disturbance. While optimization approach is implemented for both radial and mesh networks to minimize the network transmission loss, such that considering the communication infrastructure, the optimization approach achieves OPF under steady-state network operation. These concepts are investigated and deployed with modified CIGRE B4 network as a benchmark. The modified CIGRE B4 cases results have shown the required adjustments for the droop gains in the radial network and the mesh network operating voltages to achieve minimum transmission loss. This study showed general approaches for efficient power flow with minimum power loss in a generalized MTDC network configuration under normal network operation.

6. Declarations of interest

None.

Acknowledgments

This publication was made possible by NPRP grant NPRP (9-092-2-045) from the Qatar National Research Fund (a member of Qatar Foundation). The statements made herein are solely the responsibility of the authors.

References

[1] P. Wang, L. Goel, X. Liu, F.H. Choo, Harmonizing AC and DC: A hybrid AC/DC future grid solution, IEEE Power Energy Mag. 11 (2013) 76–83, https://doi.org/10.1109/MPE.2013.2245587.

[2] M. Hajian, L. Zhang, D. Jovcic, DC transmission grid with low-speed protection using mechanical DC circuit breakers, IEEE Trans. Power Deliv. 30 (2015) 1383–1391, https://doi.org/10.1109/TPWRD.2014.2371618.

[3] B.K.J. Michael, P. Bahrman, The ABCs of HVDC transmission technologies, IEEE Power Energy Mag. (2007) 32–44.

[4] N.R. Chaudhuri, B. Chaudhuri, R. Majumder, A. Yazdani, Multi-terminal direct-current grids modeling, analysis, and control, 2014. https://doi.org/10.1016/j.brainres.2006.05.016.
[5] M. Eremia, R. Mihalic, B. Blazic, Advanced solutions in power systems HVDC, FACTS, and Artificial Intelligence, 2016. https://doi.org/10.1002/9781119175391.
[6] H. Rao, Architecture of Nan'ao multi-terminal VSC-HVDC system and its multi-functional control, CSEE J. Power Energy Syst. 1 (2015) 9–18.
[7] M.R. Banaei, E. Salary, Mitigation of voltage sag, swell and power factor correction using solid-state transformer based matrix converter in output stage, Alexandria Eng. J. 53 (2014) 563–572, https://doi.org/10.1016/j.aej.2014.06.003.
[8] K. Thakre, K.B. Mohanty, A. Chatterjee, Reduction of circuit devices in symmetrical voltage source multilevel inverter based on series connection of basic unit cells, Alexandria Eng. J. 57 (4) (2018) 2703–2712, https://doi.org/10.1016/j.aej.2017.11.001.
[9] M.R. Banaei, A. Fazel Bakhshayesh, Selection of DC voltage magnitude using Fibonacci series for new hybrid asymmetrical multilevel inverter with minimum PIV, Alexandria Eng. J. 53 (2014) 529–535, https://doi.org/10.1016/j.aej.2014.06.008.
[10] M. Ahmed, A. Sheir, M. Orabi, Asymmetric cascaded half-bridge multilevel inverter without polarity changer, Alexandria Eng. J. 57 (4) (2018) 2415–2426, https://doi.org/10.1016/j.aej.2017.08.018.
[11] E. Pierri, O. Binder, N.G.A. Hemdan, M. Kurrat, Challenges and opportunities for a European HVDC grid, Renew. Sustain. Energy Rev. 70 (2017) 427–456, https://doi.org/10.1016/j.rser.2016.11.233.
[12] S. Taggart, G. James, Z. Dong, C. Russell, The future of renewables linked by a transnational Asian grid, Proc. IEEE. 100 (2012) 348–359, https://doi.org/10.1109/JPROC.2011.2159089.
[13] A. Einsiedler, Enabling DESERTEC in EUMENA - Deutsche Bank, (n.d.). http://www.solarmillennium.de/includes/force_download.php?client=1&path=upload/Download/Unternehmen/eng/Dii_Brochure_as_of_February2010.pdf.
[14] M. Ram, D. Bogdanov, A. Aghahosseini, S. Oyewo, A. Gulagi, M. Child, C. Breyer, H.-J. Fell, Global energy system based on 100% renewable energy – Power Sector, Berlin, 2017.
[15] A. Egea-Alvarez, J. Beerten, D. Van Hertem, O. Gomis-Bellmunt, Hierarchical power control of multiterminal HVDC grids, Electr. Power Syst. Res. 121 (2015) 207–215, https://doi.org/10.1016/j.epsr.2014.12.014.
[16] P. Rodriguez, A. Luna, W. Zhang, G.B. Gharehpetian, K. Rouzbehi, Multi-terminal HVDC grids with inertia mimicry capability, IET Renew. Power Gener. 10 (2016) 752–760, https://doi.org/10.1049/iet-rpg.2015.0463.
[17] K. Rouzbehi, A. Miranian, J.I. Candela, A. Luna, P. Rodriguez, A hierarchical control structure for multi-terminal VSC-based HVDC grids with GVD characteristics, Proc. 2013 Int. Conf. Renew. Energy Res. Appl. ICRERA 2013 (2013) 996–1001, https://doi.org/10.1109/ICRERA.2013.6749897.
[18] C. Gavriluta, I. Candela, A. Luna, A. Gomez-Exposito, P. Rodriguez, Hierarchical control of HV-MTDC systems with droop-based primary and OPF-based secondary, IEEE Trans. Smart Grid. 6 (2015) 1502–1510, https://doi.org/10.1109/TSG.2014.2365854.
[19] M.A. Abdelwahed, E.F. El-Saadany, Power sharing control strategy of multiterminal VSC-HVDC transmission systems utilizing adaptive voltage droop, IEEE Trans. Sustain. Energy. 8 (2017) 605–615, https://doi.org/10.1109/TSTE.2016.2614223.
[20] A. Benchaib, Advance control of AC-DC power networks system of systems approach based on spatio-temporal scales, London, 2015.
[21] A.S. Abdel-Khalik, A.M. Massoud, A.A. Elserougi, S. Ahmed, Optimum power transmission-based droop control design for multi-terminal HVDC of offshore wind farms, IEEE Trans. Power Syst. 28 (2013) 3401–3409, https://doi.org/10.1109/TPWRS.2013.2238685.
[22] N. Flourentzou, V.G. Agelidis, G.D. Demetriades, VSC-based HVDC power transmission systems: An overview, IEEE Trans. Power Electron. 24 (2009) 592–602, https://doi.org/10.1109/TPEL.2008.2008441.
[23] X. Zhao, K. Li, M. Zheng, Analysis of transmission loss in droop control of a multi-terminal HVDC system, J. Power Energy Eng. 02 (2014) 564–572, https://doi.org/10.4236/jpee.2014.24076.
[24] Y. Wang, W. Wen, C. Wang, H. Liu, X. Zhan, X. Xiao, Adaptive voltage droop control of multiterminal VSC-HVDC systems for DC voltage deviation and power sharing, IEEE Trans. Power Deliv. 8977 (2018) 1–8, https://doi.org/10.1109/TPWRD.2018.2844330.
[25] J. Beerten, R. Belmans, Analysis of power sharing and voltage deviations in droop-controlled DC grids, IEEE Trans. Power Syst. 28 (2013) 4588–4597, https://doi.org/10.1109/TPWRS.2013.2272494.
[26] J. Khazaei, Z. Miao, L. Piyasinghe, L. Fan, Minimizing DC system loss in multi-terminal HVDC systems through adaptive droop control, Electr. Power Syst. Res. 126 (2015) 78–86, https://doi.org/10.1016/j.epsr.2015.04.020.
[27] F.D. Bianchi, O. Gomis-Bellmunt, Droop control design for multi-terminal VSC-HVDC grids based on LMI optimization, Proc. IEEE Conf. Decis. Control. (2011) 4823–4828, https://doi.org/10.1109/CDC.2011.6161070.
[28] J. Beerten, R. Eriksson, R. Belmans, Influence of DC voltage droop settings on AC system stability, 10th IET Int Conf. AC DC Power Transm. (ACDC) 2012 (2012) (2012) 13, https://doi.org/10.1049/cp.2012.1960.
[29] N.R. Chaudhuri, B. Chaudhuri, Adaptive droop control for effective power sharing in multi-terminal DC (MTDC) grids, IEEE Trans. Power Syst. 28 (2013) 21–29, https://doi.org/10.1109/TPWRS.2012.2203390.
[30] M. Aragüés-Peñalba, A. Egea-Àlvarez, O. Gomis-Bellmunt, A. Sumper, Optimum voltage control for loss minimization in HVDC multi-terminal transmission systems for large offshore wind farms, Electr. Power Syst. Res. 89 (2012) 54–63, https://doi.org/10.1016/j.epsr.2012.02.006.
[31] M. Aragüés-Peñalba, A. Egea-Àlvarez, S.G. Arellano, O. Gomis-Bellmunt, Droop control for loss minimization in HVDC multi-terminal transmission systems for large offshore wind farms, Electr. Power Syst. Res. 112 (2014) 48–55, https://doi.org/10.1016/j.epsr.2014.03.013.
[32] E. Prieto-Araujo, F.D. Bianchi, A. Junyent-Ferre, O. Gomis-Bellmunt, Methodology for droop control dynamic analysis of multiterminal VSC-HVDC grids for offshore wind farms, IEEE Trans. Power Deliv. 26 (2011) 2476–2485, https://doi.org/10.1109/TPWRD.2011.2144625.
[33] K. Li, X. Zhao, Adaptive backstepping droop controller design for multi-terminal high-voltage direct current systems, IET Gener. Transm. Distrib. 9 (2015) 975–983, https://doi.org/10.1049/iet-gtd.2014.0582.
[34] E. Prieto-Araujo, A. Egea-Alvarez, S. Fekriasl, O. Gomis-Bellmunt, DC voltage droop control design for multiterminal HVDC systems considering AC and DC grid dynamics, IEEE Trans. Power Deliv. 31 (2016) 575–585, https://doi.org/10.1109/TPWRD.2015.2451531.
[35] R. Teixeira Pinto, P. Bauer, S.F. Rodrigues, E.J. Wiggelinkhuizen, J. Pierik, B. Ferreira, A novel distributed direct-voltage control strategy for grid integration of offshore wind energy systems through MTDC network, IEEE Trans. Ind. Electron. 60 (2013) 2429–2441, https://doi.org/10.1109/TIE.2012.2216239.
[36] M. Aragüés-Peñalba, J. Sau Bassols, S. Galceran Arellano, A. Sumper, O. Gomis Bellmunt, Optimal operation of hybrid high voltage direct current and alternating current networks based on OPF combined with droop voltage control, Int. J. Electr. Power

Energy Syst. 101 (2018) 176–188, https://doi.org/10.1016/j.ijepes.2018.03.010.
[37] M. Han, D. Xu, L. Wan, Hierarchical optimal power flow control for loss minimization in hybrid multi-terminal HVDC transmission system, CSEE J. Power Energy Syst. 2 (2016) 40–46, https://doi.org/10.17775/CSEEJPES.2016.00007.
[38] T. An, C. Han, Y. Wu, G. Tang, HVDC grid test models for different application scenarios and load flow studies, J. Mod. Power Syst. Clean Energy. 5 (2017) 262–274, https://doi.org/10.1007/s40565-016-0214-7.
[39] T. An, X. Zhou, C. Han, Y. Wu, A DC grid benchmark model for studies of interconnection of power systems, CSEE J. Power Energy Syst. 1 (2015) 101–109, https://doi.org/10.17775/CSEEJPES.2015.00053.
[40] S. Li, T.A. Haskew, L. Xu, Control of HVDC light system using conventional and direct current vector control approaches, IEEE Trans. Power Electron. 25 (2010) 3106–3118, https://doi.org/10.1109/TPEL.2010.2087363.
[41] M.M. Ismail, A.F. Bendary, Protection of DFIG wind turbine using fuzzy logic control, Alexandria Eng. J. 55 (2016) 941–949, https://doi.org/10.1016/j.aej.2016.02.022.
[42] E.G. Shehata, Sliding mode direct power control of RSC for DFIGs driven by variable speed wind turbines, Alexandria Eng. J. 54 (2015) 1067–1075, https://doi.org/10.1016/j.aej.2015.06.006.
[43] L.X.L. Yao, DC voltage control and power dispatch of a multi-terminal HVDC system for integrating large offshore wind farms, IET Renew. Power Gener. 5 (2011) 223–233, https://doi.org/10.1049/iet-rpg.2010.0118.
[44] J. Cao, W. Du, H.F. Wang, S.Q. Bu, Minimization of transmission loss in meshed AC/DC grids with VSC-MTDC networks, IEEE Trans. Power Syst. 28 (2013) 3047–3055, https://doi.org/10.1109/TPWRS.2013.2241086.
[45] M.J. Carrizosa, F.D. Navas, G. Damm, F. Lamnabhi-Lagarrigue, Optimal power flow in multi-terminal HVDC grids with offshore wind farms and storage devices, Int. J. Electr. Power Energy Syst. 65 (2015) 291–298, https://doi.org/10.1016/j.ijepes.2014.10.016.
[46] S.E. De Leon-Aldaco, H. Calleja, J. Aguayo Alquicira, Metaheuristic optimization methods applied to power converters: A review, IEEE Trans. Power Electron. 30 (2015) 6791–6803, https://doi.org/10.1109/TPEL.2015.2397311.
[47] X.-S. Yang, Engineering optimization: an introduction with metaheuristic applications, 2010. https://doi.org/10.1002/9780470640425.
[48] M.J. Mahmoodabadi, A.R. Ghavimi, S.M.S. Mahmoudi, Optimization of power and heating systems based on a new hybrid algorithm, Alexandria Eng. J. 54 (2015) 343–350, https://doi.org/10.1016/j.aej.2015.04.011.
[49] S. Harish Kiran, S.S. Dash, C. Subramani, Performance of two modified optimization techniques for power system voltage stability problems, Alexandria Eng. J. 55 (2016) 2525–2530, https://doi.org/10.1016/j.aej.2016.07.023.